Transfer of Orbital Angular Momentum to Freely Levitated High-Density Objects in Airborne Acoustic Vortices

B.W. Zhang,[1] Z.Y. Hong,[1,*] and B.W. Drinkwater[2]

[1] *MOE Key Laboratory of Materials Physics and Chemistry under Extraordinary Conditions, School of Physical Science and Technology, Northwestern Polytechnical University, Xi'an 710072, China*

[2] *Department of Mechanical Engineering, University Walk, University of Bristol, Bristol BS8 1TR, United Kingdom*

Vortex-field acoustic levitation is an application of acoustic vortices that allows the manipulation of a wide range of materials in various media. However, to date, its levitation capability in air is limited to relatively low-density objects. Here, by optimizing an array-tube setup, we levitate iridium (22.56 g/cm^3) in a first-order acoustic vortex in air. This technique makes it possible to observe the orbital angular momentum transfer carried by acoustic vortices to freely levitated high-density objects, of which the highest rotation speed reaches up to 6500 revolutions per second and increases with a decrease in the object size and an increase in the source amplitude. It is revealed that the thermal-viscous boundary layer dissipation is the dominant effect and leads directly to the rapid rotation of high-density objects. This work can expand the application scope of acoustic vortices, especially in the fields of containerless processing of various materials and rapid rotation of objects, and help to understand the mechanisms of orbital angular momentum transfer to matter.

I. INTRODUCTION

Vortices have been shown to exist in acoustics [1], optics [2], and even quantum mechanics [3]. They are characterized by helicoidal wave fronts, null-pressure centers, and carry orbital angular momentum (OAM), and thus, have found application in manipulating objects [4,5] and even communication [6,7]. Compared with optical vortices, acoustic vortices can provide a larger trapping force and higher driving torque to objects of different scales without limitation on their electromagnetic properties [8], and hence, are widely applicable across fields such as containerless processing of various materials [9,10], rotation of objects [11,12], and biomedical research [13] in the ground and space environments.

Recent works showed that an array of individually addressed sources excited with appropriate phases could generate acoustic vortices of different orders (topological charges, $m > 0$) and be applied to manipulate objects [14–19]. For example, Seah *et al.* used an eight-element circular array to trap and move expanded polystyrene spheres in air [17]. Thereafter, Hong *et al.* employed a small number of peripherally placed piezoelectric sources to stably levitate water drops and observe their dynamic motions [18]. However, these experiments in air concerned only objects with a density no more than water (1 g/cm^3). To resolve

this issue, Hong *et al.* proposed a method to generate strong acoustic vortices by using an array-tube configuration and successfully levitated metal materials [19]. Nevertheless, the vortex-field acoustic levitation (VFAL) of high-density matter, such as iridium (22.6 g/cm^3), has not yet been realized, although it has been realized in a standing-wave acoustic levitator with $m = 0$ [20]. By realizing this, the application scope of VFAL can be greatly expanded.

The transfer of acoustic OAM to matter is experimentally observed and can be classified into three mechanisms, according to the type of matter and modes of interaction between matter and the acoustic field. In the first category, OAM transfer is mainly to bulk absorption of acoustic power and leads to low-speed rotation of large-size (relative to wavelength) solid disks restrained by a string or rod. For example Volke-Sepulveda *et al.* [21] and Skeldon *et al.* [22] used circular arrays of individually addressed loudspeakers to generate acoustic vortices in air and a torsion pendulum to study OAM transfer to hanging disks. Demore *et al.* used an array with 1000 addressable sources and a rod-stabilized disk in water to demonstrate that the ratio between the OAM flux and the acoustic power is equal to the ratio of the topological charge of an acoustic helicoidal beam and its angular frequency [23]. Anhauser *et al.* spun a disk in viscous liquids using an ultrasonic vortex beam to demonstrate the balance between the acoustic radiation torque and the viscous torque [24]. In the second category, OAM is transferred to an absorbing liquid. This

*hongzy@nwpu.edu.cn

was theoretically estimated by Anhauser *et al.* [24] and Riaud *et al.* [25], and experimentally evidenced by Hong *et al.* [26]. The effect results in a slow swirling of liquid about the vortex axis, in which the motion follows the OAM density distribution. The third category concerns both OAM transfer to trapped particles and the host liquid in acoustic vortices. For example, Baresch and Thomas observed OAM transfer to stably trapped elastic particles in a liquid, in which the acoustic bulk absorption of particles, the viscous boundary-layer dissipation of the surrounding fluid and the external rotational steady flow all contribute to the low-speed rotation of particles [27]. However, OAM transfer to stably trapped high-density objects by acoustic vortices in air has never been observed before.

Because gas media have lower dynamic viscosities than that of liquids at common pressure and temperature, acoustic OAM transfer to levitated objects in air is expected to achieve rapid rotation of objects, which can create extreme conditions for testing material properties [28,29]. Compared to optical and magnetic-rotation-driving techniques, which can work in vacuum [28,30,31], VFAL works in gas medium, and hence, any rotating objects experience aerodynamic drag, which can be expected to limit the highest rotation speed. Nevertheless, VFAL can levitate objects with larger masses and sizes than other techniques, which can allow objects such as microchips to be levitated and x-ray or other spectroscopic characterization to be performed during rapid rotation.

Here, the optimal configuration parameters of an array-tube setup are explored to enhance the levitation capability of first-order acoustic vortices. This method generates high acoustic pressures by exciting resonances of the cylindrical cavity, which amplify the outputs of the sources. Based on this apparatus, VFAL of iridium is demonstrated and the rapid-rotation phenomenon of OAM transfer from acoustic vortices to freely levitated high-density objects is then observed. Thereafter, the drag torques exerted on the rapid-rotation objects by air under high Reynolds numbers are numerically evaluated according to the theory of fluid dynamics, and the driving torques arising from OAM transfer are uncovered by utilizing the thermal-viscous boundary-layer dissipation theory. A numerical simulation of microparticle rotation by acoustic radiation torque under relatively low rotation speeds and Reynolds numbers can be found in Ref. [32].

II. EXPERIMENTAL SETUP AND PARAMETER OPTIMIZATION

Previous work demonstrated that using a tube with appropriate geometric parameters to constrain the acoustic field could excite resonant modes of a cylindrical cavity and greatly increase the levitation capability of cylindrical standing-wave traps [19,33]. Motivated by that, an array-tube setup is designed and built in this work to achieve a
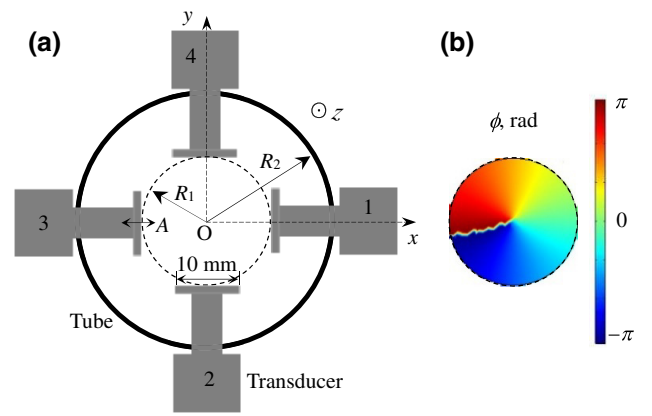

FIG. 1. Array-tube setup and generated first-order acoustic vortices. (a) Schematic of an acoustic array constituted by four peripherally and uniformly placed piezoelectric transducers and a coaxial tube (top view). (b) Phase, ϕ, distribution of the first-order acoustic vortices in the x-y plane. The z axis is along the vortex axis, parallel to the direction of gravity.

more powerful levitation capability, as shown in Fig. 1(a). It is made up of four peripherally and uniformly placed piezoelectric acoustic sources coaxial with a tube. All sources have a circular cross-section diameter of 10 mm and a separation radius of R_1 to the setup center. They can vibrate at the same frequency of 23 kHz (wavelength, $\lambda = 14.9$ mm) and the same surface vibration amplitude of A, adjustable from 0 to 25 μm. The control accuracy of A is about ±0.5 μm. Different phases can be applied to each source to generate the first-order Bessel-shaped acoustic vortices ($m = \pm1$, M1 within the Supplemental Material [34]) [35–37], as shown in Fig. 1(b). The tube has an inner radius of R_2 and a height of 50 mm. This height is preset to facilitate the experimental operation and reduce the number of free variables in the following optimization calculations. The setup works in air at a controlled environment temperature of 20 °C and the corresponding density, ρ, and sound speed, c, of air are 1.2×10^{-3} g/cm³ and 343 m/s, respectively. A laser displacement sensor (Keyence LK-H008W) is used to measure the vibration amplitude, A, of each source.

To achieve the best levitation performance, the theoretical optimization of R_1 and R_2 is implemented by modeling the experimental setup in the acoustics module of COMSOL Multiphysics. As the deepest potential wells (i.e., strongest trapping forces) lie in the vortex center of the first-order acoustic vortices [19], the Gor'kov potential values [38], U_c, of the vortex (setup) center with the change of R_1 and R_2 are calculated (M2 within the Supplemental Material [34]), as shown in Fig. 2(a). It can be seen that the lowest values of U_c, namely, the deepest potential wells, appear around $R_1 = 0.35\lambda$ and $R_2 = 0.75\lambda$, 1.26λ, 1.80λ, etc. In these cases, the acoustic pressures, p, in the array-tube setup can be higher than 10^4 Pa as A approaches 20 μm.
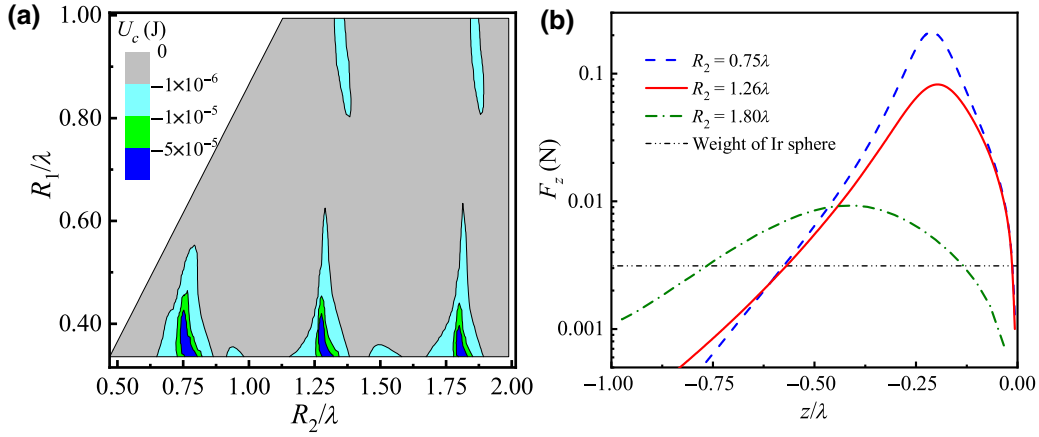
FIG. 2. Parameter optimization of the array-tube setup. (a) Gor'kov potential values, U_c, of the vortex center at different configuration parameters of R_1 and R_2. (b) Acoustic radiation forces, F_z, exerted on an iridium sphere as it moves along the z axis at $R_1 = 0.35\lambda$. In (a),(b), it is assumed that the sphere in the acoustic field has a radius of 1.5 mm. In (b), the weight of a 1.5-mm-radius iridium sphere is drawn for comparison. Vibration amplitude, A, of each source is 20 μm in these calculations.

Accordingly, the acoustic radiation forces, F_z, exerted by the resonant acoustic fields on an iridium sphere (radius, $a = 1.5$ mm) when it moves along the vortex axis (z axis) are calculated (M3 within the Supplemental Material [34]) [8,39], as shown in Fig. 2(b). It can be seen that, for the optimal configuration parameters of R_1 and R_2, the vortex center of the first-order acoustic vortices generated by the array-tube setup with four sources can theoretically provide a sufficient acoustic radiation force to levitate iridium, and hence, other high-density substances.

III. VORTEX-FIELD ACOUSTIC LEVITATION OF HIGH-DENSITY OBJECTS

Based on the above optimal parameters, a tube with an inner radius of 18.8 mm (1.26λ) is designed and made to construct the array-tube setup with four sources (Fig. S1 within the Supplemental Material [34]). Thereafter, by, respectively, adjusting the separation radius, R_1, of each source to 5.2 mm (0.35λ) and the vibration amplitude, A, to adequate values, high-density objects, including a steel sphere (7.9 g/cm^3), a brass sphere (8.7 g/cm^3), and an iridium sphere (22.56 g/cm^3), are successfully levitated in the vortex center of the first-order acoustic vortices, as shown in Fig. 3 (Movie 1 within the Supplemental Material [34]).

IV. OBSERVATION OF HIGH-SPEED ROTATION MOTIONS

Here, the optimized array-tube setup makes it possible to observe the phenomenon of OAM transfer from acoustic vortices to any freely levitated high-density objects in air. By employing an ultrahigh-speed camera, able to work above 5×10^4 frames per second (Fastcam Mini AX200), the high-speed rotation motions of the steel and brass spheres at $A = (15 \pm 0.5)$ μm and the iridium spheres

at $A = (20 \pm 0.5)$ μm are recorded (M4 and Movies 2–4 within the Supplemental Material [34]). From the movies, we can see that the rotation motions of the spheres are around the vortex axis (z axis) and their rotation directions coincide with the chirality of the first-order acoustic vortices. The rotation speeds of the steel, brass, and iridium spheres with different radii are extracted from the movies and plotted in Fig. 4. It can be seen that the rotation rate, Ψ, of a sphere increases with a decrease in the sphere radius, a, and an increase in each source amplitude, A. This is independent of the material of the objects, which is very different from the optical or magnetic driving cases where objects with special electromagnetic properties are required [28,30,31]. In the experiments, the highest rotation speed of the spheres reaches up to 6500 revolutions per second (rps), which is 2 orders of magnitude higher than that of the acoustically trapped particles in water [26,27] and still 3 orders of magnitude lower than that of the optically levitated particles under vacuum [30,31]. The corresponding highest circumferential speed and centrifugal acceleration of these spheres reach up to 50 m/s and 2×10^6 m/s^2, respectively. We speculate that these rotational rates can be further increased by reducing the size of object, raising the intensity of acoustic vortices and decreasing the viscosity of gas medium (such as by lowering temperature).

V. DRAG TORQUES UNDER HIGH REYNOLDS NUMBERS

The rotation motions of the freely levitated high-density objects are controlled by the balance between the drag torque, Γ_D, from air and the acoustic radiation torque, Γ_A, from OAM transfer. However, due to the high densities and
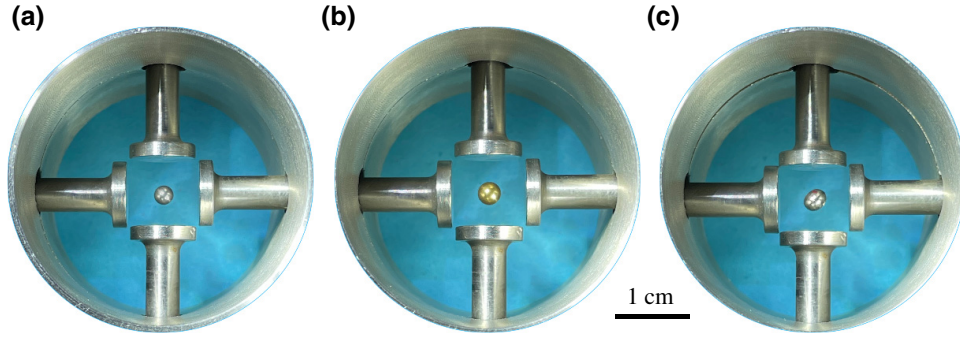
FIG. 3.　Vortex-field acoustic levitation of high-density objects (top view): (a) steel sphere (7.9 g/cm^3), (b) brass sphere (8.7 g/cm^3), and (c) iridium sphere (22.56 g/cm^3).

rotation speeds of the objects, the physical mechanisms need to be more deeply analyzed.

First, the Reynolds numbers associated with the high-speed rotation of the spheres in air are calculated by $\mathrm{Re} = \rho a^2 \Omega / \eta$, where a is the radius of a sphere, $\Omega = 2\pi\Psi$ is the angular speed of a sphere, and η is the dynamic viscosity of air (Fig. S2 within the Supplemental Material [34]). The magnitude of Re is about 10^3, which is much higher than 1. Obviously, the Stoke's drag expression, $\Gamma_D = -8\pi\eta a^3 \Omega$, for the drag torque on a rotational sphere at low Re ($\ll 1$) is not applicable here (Supplemental Material Fig. S3 [34]). According to the study in Ref. [40], the laminar-to-turbulence transition around a sphere surface occurs at Re values of 10^5 ($\gg 10^3$). Therefore, the full steady-state Navier-Stokes equation can be solved numerically to find Γ_D without considering possible turbulence.

Because the magnitude of sound pressure here (10^4 Pa) is less than one standard atmosphere and frictional drag emerges, the air can be regarded as an incompressible viscous fluid in this study. In this case, the steady-state

equation of fluid motion is in the form (see Eq. (15.7) in Ref. [41])

$$\rho(\mathbf{v}' \cdot \nabla)\mathbf{v}' = -\nabla p' + \eta\Delta\mathbf{v}', \tag{1}$$

where p' is the hydrodynamic pressure and $\mathbf{v}'$ is the fluid velocity. If we take spherical polar coordinates (r, θ, ϕ) with the polar axis parallel to the rotational axis of a sphere, we have $v_r' = v_\theta' = 0$ and $v_\phi' = v'$. Thus, the frictional force on unit area of the sphere is $\sigma_{r,\phi} = \eta((\partial v'/\partial r) - v'/r)_{r=a}$ and the resulting drag torque can be obtained from $\Gamma_D = \int_0^\pi \sigma_{r,\phi} 2\pi a^3 \sin\theta\, d\theta$. Because it is hard to find the analytical solution of Eq. (1), we numerically solve it with the experimental boundary conditions $v'|_{r=a} = a\Omega$ and $v'|_{r=R_1} = 0$ in the commercial software ANSYS Fluent 2021 R1. As a result, the drag torques corresponding to spheres with different radii and rotation speeds in Fig. 4 are predicted, as plotted in Fig. 5. The uncertainties of Γ_D are caused by the measurement errors of a and Ψ. It can be found that the drag torques increase initially and decrease afterwards with an increase of the sphere radius, and the highest torque reaches up to 4×10^{-7} N m.
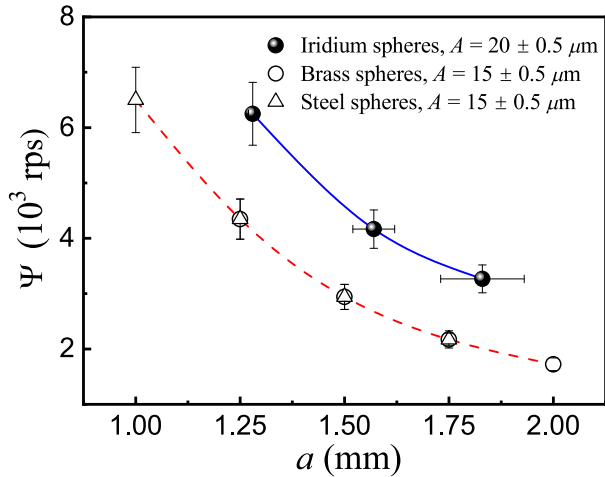
VI. MECHANISMS OF OAM TRANSFER

It is known that OAM transfer via the acoustic radiation torque exerted on an object by acoustic vortices is $\Gamma_A = (m/\omega)P_{\mathrm{abs}}$ [42], where m is the vortex order (topological charge) and ω is the angular frequency of the acoustic waves; P_{abs} is the total acoustic power absorbed by an object, including the bulk absorption and the acoustic boundary-layer dissipation. At first, to evaluate the contribution of bulk absorption, we calculate the acoustic energy density, E_{Ir}, within the centrally located iridium sphere as well as the acoustic energy density, E_{air}, in the surrounding air and find that the ratio of $E_{\mathrm{Ir}}/E_{\mathrm{air}}$ is about 10^{-4}, revealing that the majority of the acoustic energy is in the air (Fig. S4 within the Supplemental Material [34]). The same rotation speeds of the steel and brass spheres at the same radii in Fig. 4 verify that the steel and brass materials make little difference to the rotation speeds. Therefore, it can be
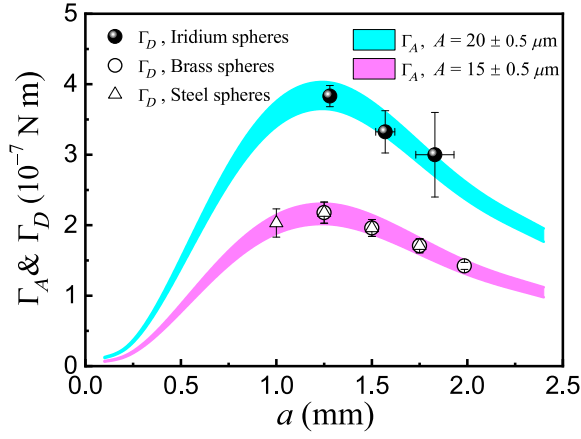

FIG. 4.　Experimental rotation rates, Ψ, versus the sphere radii, a.

FIG. 5. Drag torques, Γ_D, from air under high Reynolds numbers and acoustic radiation torques, Γ_A, from OAM transfer contributed by the thermal-viscous boundary-layer dissipation.

deduced that, for high-density spheres in airborne acoustic vortices, the contribution of bulk absorption to the driving torque is negligible.

Next, to evaluate the contribution of the boundary-layer dissipation, the thermal and viscous dissipation of the acoustic boundary layers surrounding a centrally located sphere should be included in the calculation of acoustic field. Generally, this needs time- and resource-consuming solutions of the linearized compressible Navier-Stokes equations. Now, it can be realized at a low cost by using a thermal-viscous boundary-layer impedance condition on the object's surface [43]. The core strategy of this method is that the viscous and thermal boundary-layer effects can be represented as a boundary condition on the standard Helmholtz equation for acoustic pressure, which is

$$-\delta_v \frac{i-1}{2} \Delta_T p + \delta_{\text{th}} k_0^2 \frac{(i-1)(\gamma-1)}{2} p + \frac{\partial p}{\partial n} = 0 \quad (2)$$

on a wall, where $\delta_v = \sqrt{2\eta/\omega\rho}$ is the thicknesses of the viscous boundary layer and $\delta_{\text{th}} = \sqrt{2\kappa/\omega\rho c_p}$ is the thicknesses of the thermal boundary layer. In Eq. (2), Δ_T is the projection of the Laplace operator on the wall, κ is the coefficient of thermal conductivity, $k_0 = \omega/c$ is the isentropic wave number, $\gamma = c_p/c_V$ is the specific heat ratio, and $\mathbf{n}$ is the normal field vector. The boundary-layer impedance condition allows for some slip velocity along the normal direction to the sphere ($v_n \neq 0$, see Eq. (23) in Ref. [43]). This method is verified to be highly effective when the wavelength and the minimum radius of curvature of the wall is much larger than the boundary-layer thickness. In this study, the acoustic wavelength is about 14.9 mm and the diameters of the spheres are around 3 mm, which are much larger than $\delta_v \approx 14$ μm and $\delta_{\text{th}} \approx 500$ μm, hence meeting the applicable conditions. Because the method is integrated into the acoustics

module of COMSOL Multiphysics, what we need to do during the calculation of total acoustic field (p and $\mathbf{v}$) is to set the thermal-viscous boundary-layer impedance condition on the sphere surface in the physical model of an array-tube setup with a centrally located sphere (Fig. S5 within the Supplemental Material [34]). After obtaining acoustic pressure, p, and fluid particle velocity, $\mathbf{v}$, of the total acoustic field, the acoustic radiation torque exerted on the sphere can be obtained from $\Gamma_A = \iint_{S_R} - \langle \mathbf{r} \times \Pi \rangle \, dS_R$, where $\Pi = (p + P)\mathbf{I} + \rho\mathbf{vv}$ is the acoustic momentum flux density tensor, $P = -\rho v^2/2 + p^2/2\rho c^2$ is the second-order acoustic radiation pressure, $\mathbf{r}$ is the vector position from the center of the sphere to a point in space, $\mathbf{I}$ is the unit tensor, S_R is the virtual sphere surface enclosing the real sphere, and the symbol $\langle \ \rangle$ denotes time averaging over a period of acoustic vibration [42,44,45]. Considering $\iint_{S_R} - \langle (p + P)\mathbf{r} \times \mathbf{I} \rangle \, dS_R = 0$ and that the acoustic field here is axisymmetric, Γ_A is along the z axis and can be reduced to $\Gamma_A = \iint_{S_R} -\rho \langle (\mathbf{r} \times \mathbf{v})_z v_n \rangle \, dS_R$, where v_n is the outward velocity normal to the sphere surface (see Eq. (8) in Ref. [42] or Eq. (4) in Ref. [45]). Consequently, the driving torques of Γ_A with a change to the sphere radius, a, around the source vibration amplitudes, $A = 15$ and 20 μm, are simulated, as plotted also in Fig. 5. The uncertainties of Γ_A are induced by the control errors of A (± 0.5 μm). It can be seen that the predicted driving torques, Γ_A, coincide well with the drag torques, Γ_D, quantitatively, indicating that the boundary-layer dissipation is the dominant mechanism of OAM transfer here.

VII. CONCLUSION

In the field of acoustic levitation, only standing waves with zero topological charge are capable of levitating high-density materials, such as iridium, for containerless processing [20]. Here, the VFAL of iridium (22.56 g/cm^3) in air is realized by optimizing an array-tube setup with four sources to generate the first-order acoustic vortices. We optimize the array-tube setup by adjusting the separation radius of the sources and the inner radius of the tube to produce high levitation forces. This optimization is performed in simulations, based on the Gor'kov potential, and is used to design an experimental apparatus.

We note that the previous observations of acoustic OAM transfer to matter in water systems lead to rotation speeds of about 10^1 rps [26,27]. In this study, the high-speed rotation (6500 rps) of the freely levitated high-density objects in acoustic vortices in air is observed, which is 2 orders of magnitude higher than previous observations, mainly due to the lower dynamic viscosity (1.79×10^{-5} Pa s) of air than that (1.01×10^{-3} Pa s) of water. It is found that the rotation speed of a high-density object in the first-order acoustic vortices increases with a decrease in the object size and an increase in the source amplitude, and this is independent of the material of the object. Theoretical

analyses indicate that the high-speed rotation of a high-density object is mainly caused by OAM transfer from the dissipation of the thermal-viscous boundary layers surrounding the object's surface. It should also be noted that, in this study, the drag torque exerted on an object by air is analyzed under high Reynolds numbers (10^3) without considering possible turbulence. However, the Reynolds-averaged Navier-Stokes equation may be solved in future research to consider turbulence.

ACKNOWLEDGMENTS

[1] J. F. Nye and M. V. Berry, Dislocations in wave trains, Proc. R. Soc. A **336,** 165 (1974).

[2] P. Coullet, L. Gil, and F. Rocca, Optical vortices, Opt. Commun. **73,** 403 (1989).

[3] A. Luski, Y. Segev, R. David, O. Bitton, H. Nadler, A. R. Barnea, A. Gorlach, O. Cheshnovsky, I. Kaminer, and E. Narevicius, Vortex beams of atoms and molecules, Science **373,** 1105 (2021).

[4] S. Franke-Arnold, L. Allen, and M. Padgett, Advances in optical angular momentum, Laser Photonics Rev. **2,** 299 (2008).

[5] A. Marzo and B. W. Drinkwater, Holographic acoustic tweezers, Proc. Natl. Acad. Sci. U. S. A. **116,** 84 (2019).

[6] N. Bozinovic, Y. Yue, Y. X. Ren, M. Tur, P. Kristensen, H. Huang, A. E. Willner, and S. Ramachandran, Terabit-scale orbital angular momentum mode division multiplexing in fibers, Science **340,** 1545 (2013).

[7] C. Shi, M. Dubois, Y. Wang, and X. Zhang, High-speed acoustic communication by multiplexing orbital angular momentum, Proc. Natl. Acad. Sci. **114,** 7250 (2017).

[8] M. Baudoin and J.-L. Thomas, Acoustic tweezers for particle and fluid micromanipulation, Annu. Rev. Fluid Mech. **52,** 205 (2020).

[9] E. H. Brandt, Suspended by sound, Nature **413,** 474 (2001).

[10] P. C. Nordine, D. Merkley, J. Sickel, S. Finkelman, R. Telle, A. Kaiser, and R. Prieler, A levitation instrument for containerless study of molten materials, Rev. Sci. Instrum. **83,** 125107 (2012).

[11] T. G. Wang, E. H. Trinh, A. P. Croonquist, and D. D. Elleman, Shapes of Rotating Free Drops: Spacelab Experimental Results, Phys. Rev. Lett. **56,** 452 (1986).

[12] C. L. Shen, W. J. Xie, and B. Wei, Parametrically excited sectorial oscillation of liquid drops floating in ultrasound, Phys. Rev. E **81,** 046305 (2010).

[13] T. Matsubara and K. Takemura, Containerless bioorganic reactions in a floating droplet by levitation technique using an ultrasonic wave, Adv. Sci. **8,** 2002780 (2021).

[14] C. R. P. Courtney, C. E. M. Demore, H. X. Wu, A. Grinenko, P. D. Wilcox, S. Cochran, and B. W. Drinkwater, Independent trapping and manipulation of microparticles using dexterous acoustic tweezers, Appl. Phys. Lett. **104,** 154103 (2014).

[15] Z. Y. Hong, J. Zhang, and B. W. Drinkwater, On the radiation force fields of fractional-order acoustic vortices, EPL **110,** 14002 (2015).

[16] A. Marzo, M. Caleap, and B. W. Drinkwater, Acoustic Virtual Vortices with Tunable Orbital Angular Momentum for Trapping of Mie Particles, Phys. Rev. Lett. **120,** 044301 (2018).

[17] S. Seah, B. W. Drinkwater, T. Carter, R. Malkin, and S. Subramanian, Dexterous ultrasonic levitation of millimeter-sized objects in air, IEEE Trans. Ultrason. Ferroelect. Freq. Control **61,** 1233 (2014).

[18] Z. Y. Hong, J. F. Yin, W. Zhai, N. Yan, W. L. Wang, J. Zhang, and B. W. Drinkwater, Dynamics of levitated objects in acoustic vortex fields, Sci. Rep. **7,** 7093 (2017).

[19] Z. Y. Hong, J. F. Yin, B. W. Zhang, and N. Yan, Vortex-field acoustic levitation in tubes, J. Appl. Phys. **128,** 104901 (2020).

[20] W. J. Xie, C. D. Cao, Y. J. Lü, and B. Wei, Levitation of Iridium and Liquid Mercury by Ultrasound, Phys. Rev. Lett. **89,** 104304 (2002).

[21] K. Volke-Sepulveda, A. O. Santillan, and R. R. Boullosa, Transfer of Angular Momentum to Matter from Acoustical Vortices in Free Space, Phys. Rev. Lett. **100,** 024302 (2008).

[22] K. D. Skeldon, C. Wilson, M. Edgar, and M. Padgett, An acoustic spanner and its associated rotational Doppler shift, New J. Phys. **10,** 013018 (2008).

[23] C. E. M. Demore, Z. Y. Yang, A. Volovick, S. Cochran, M. P. MacDonald, and G. C. Spalding, Mechanical Evidence of the Orbital Angular Momentum to Energy Ratio of Vortex Beams, Phys. Rev. Lett. **108,** 194301 (2012).

[24] A. Anhauser, R. Wunenburger, and E. Brasselet, Acoustic Rotational Manipulation Using Orbital Angular Momentum Transfer, Phys. Rev. Lett. **109,** 034301 (2012).

[25] A. Riaud, M. Baudoin, J.-L. Thomas, and O. Bou Matar, Cyclones and attractive streaming generated by acoustical vortices, Phys. Rev. E **90,** 013008 (2014).

[26] Z. Y. Hong, J. Zhang, and B. W. Drinkwater, Observation of Orbital Angular Momentum Transfer from Bessel-Shaped Acoustic Vortices to Diphasic Liquid-Microparticle Mixtures, Phys. Rev. Lett. **114,** 214301 (2015).

[27] D. Baresch and J.-L. Thomas, Orbital Angular Momentum Transfer to Stably Trapped Elastic Particles in Acoustical Vortex Beams, Phys. Rev. Lett. **121,** 074301 (2018).

[28] M. Schuck, D. Steinert, T. Nussbaumer, and J. W. Kolar, Ultrafast rotation of magnetically levitated macroscopic steel spheres, Sci. Adv. **4,** e1701519 (2018).

[29] D. Hummer, R. Lampert, K. Kustura, P. Maurer, C. Gonzalez-Ballestero, and O. Romero-Isart, Acoustic and optical properties of a fast-spinning dielectric nanoparticle, Phys. Rev. B **101,** 205416 (2020).

[30] R. Reimann, M. Doderer, E. Hebestreit, R. Diehl, and M. Frimmer, GHz Rotation of an Optically Trapped Nanoparticle in Vacuum, Phys. Rev. Lett. **121,** 033602 (2018).

[31] Y. B. Jin, J. W. Yan, S. J. Rahman, J. Li, X. D. Yu, and J. Zhang, 6 GHz hyperfast rotation of an optically levitated nanoparticle in vacuum, Photonics Res. **9,** 1344 (2021).

[32] P. Hahn, A. Lamprecht, and J. Dual, Numerical simulation of micro-particle rotation by the acoustic viscous torque, Lab Chip **16**, 4581 (2016).

[33] R. E. Apfel, A novel technique for measuring the strength of liquids, J. Acoust. Soc. Am. **49**, 145 (1971).

[34] See the Supplemental Material at http://link.aps.org/supplemental/10.1103/PhysRevApplied.18.024029 for the methods to generate acoustic vortices, calculation of the Gor'kov potential and acoustic radiation force, and supplemental figures.

[35] A. Grinenko, P. D. Wilcox, C. R. P. Courtney, and B. W. Drinkwater, Proof of principle study of ultrasonic particle manipulation by a regular-polygon array device, Proc. R. Soc. A **468**, 3571 (2012).

[36] B. T. Hefner and P. L. Marston, An acoustical helicoidal wave transducer with applications for the alignment of ultrasonic and underwater systems, J. Acoust. Soc. Am. **106**, 3313 (1999).

[37] J.-L. Thomas, J. Brunet, and F. Coulouvrat, Generalization of helicoidal beams for short pulses, Phys. Rev. E **81**, 016601 (2010).

[38] L. P. Gor'kov, On the forces acting on a small particle in an acoustical field in an ideal fluid, Sov. Phys. Dokl. **6**, 773 (1962).

[39] C. P. Lee and T. G. Wang, Acoustic radiation pressure, J. Acoust. Soc. Am. **94**, 1099 (1993).

[40] Y. Kohama and R. Kobayashi, Boundary-layer transition and the behavior of spiral vortices on rotating spheres, J. Fluid Mech. **137**, 153 (1983).

[41] L. D. Landau and E. M. Lifshitz, *Fluid Mechanics*, 2nd ed. (Pergamon Press, New York, 1987), pp. 46, 58, 65.

[42] L. K. Zhang and P. L. Marston, Angular momentum flux of nonparaxial acoustic vortex beams and torques on axisymmetric objects, Phys. Rev. E **84**, 065601 (2011).

[43] M. Berggren, A. Bernland, and D. Noreland, Acoustic boundary layers as boundary conditions, J. Comput. Phys. **371**, 633 (2018).

[44] L. Zhang and P. L. Marston, Acoustic radiation torque and the conservation of angular momentum (L), J. Acoust. Soc. Am. **129**, 1679 (2011).

[45] F. G. Mitri, T. P. Lobo, and G. T. Silva, Axial acoustic radiation torque of a Bessel vortex beam on spherical shells, Phys. Rev. E **85**, 026602 (2012).